# Modeling of Fume Formation Process in Arc Welding†

**TASHIRO Shinichi* and TANAKA Manabu****

**Abstract**

*In order to clarify fume formation mechanism in arc welding, quantitative investigation based on understanding of interaction among the electrode, arc and weld pool is indispensable. A fume formation model consisting of heterogeneous condensation model, homogeneous nucleation model and coagulation model has been developed and coupled with the GMA welding model. A series of processes from evaporation of metal vapor to fume formation from the metal vapor was totally investigated by employing this simulation model. This paper aims to visualize the fume formation process and clarify the fume formation mechanism theoretically through numerical analysis. Furthermore, the reliability of the simulation model was also evaluated through comparison of the simulation result with experimental result. As a result, it was found that most part of the fume was produced in downstream region of the arc originating from the metal vapor evaporated mainly from the droplet in argon GMA welding. This kind of the fume was constituted of particles with size of several tens nm. On the other hand, if the metal transfer becomes unstable and the metal vapor near the droplet diffuses directly toward the surroundings of the arc not getting on the plasma flow, the size of particles reaches several hundreds nm.*

**KEY WORDS:** (Simulation), (Arc), (Fume)

## 1. Introduction

In arc welding, high temperature metal vapor is generated from the melting tip of a welding wire, a droplet and a weld pool[1]. This metal vapor is cooled rapidly during diffusion to surroundings of the arc. Then primary particles of metal with 1nm~100nm in those sizes are formed through the nucleation from the metal vapor. Furthermore, a part of those particles condense and produce secondary particles with over 1 □m maximum in sizes. The particles form smoke which ascends from the arc and this phenomenon is called fume in welding[2].

Until now, most of papers show chemical composition and generation rate of the fume in comparison with welding conditions for the gas metal arc (GMA) welding because of high utilization at various manufacturing industries in the world. For example, Kobayashi *et al* observed a state of fume generation in shielded metal arc welding by employing a high speed video camera. It was qualitatively explained that metal vapor which has evaporated mainly from the droplet was released from the lower part of the arc column and generated the fume due to rapid cooling with condensation and oxidation. They also showed that amount of metal vapor from the droplet was greater than that from the weld pool[2]. Jenkins *et al* measured chemical composition of fume in shielded metal arc welding and GMA welding by Energy Dispersive Spectrometry (EDS)[3]. Bosworth *et al* discussed influence of droplet size on fume generation rate in GMA welding [4]. However, research approach to the clarifying of theoretical mechanism of fume formation is few, because the previous research approach has been almost conducted by experimental observations. In order to clarify the fume formation mechanism, it is necessary to discuss the phenomena quantitatively based on taking account of the interactions among the electrode, the arc and the weld pool. Unfortunately, phenomena in GMA welding are not fully understood due to the complex problem represented by a metal transfer.

On the other hand, theoretical research approach is advanced in the field of production of industrial nano-particles. Many researchers reported numerical simulations for clarifying the fume formation mechanism. Watanabe *et al* investigated a series of processes from evaporation of powder by thermal plasma to nucleation and condensation in cooling region for production of nano-particles in the Inductively Coupled Plasma (ICP) [5]. However, change in shape of secondary particle was not considered because of assuming all the particles to be

†Received on December 26, 2011
* Assistant professor
** Professor

Transactions of JWRI is published by Joining and Welding Research Institute, Osaka University, Ibaraki, Osaka 567-0047, Japan

spherical shape in this model. Schmid *et al* proposed a model considering change in shape of secondary particle in coagulation process, but this model was not coupled with nucleation and condensation processes[6]. From the above, there have been no research in which the whole process is totally modeled for clarifying the fume formation mechanism.

The gas tungsten arc (GTA) welding would be namely introduced to the first subject for clarifying the fume formation mechanism because of its simplified problem like a non-metal transfer. Recently, it is actively conducted to analyze the formation mechanism of the weld pool with the numerical simulation treating the electrode, the arc, and the weld pool in GTA welding as a total system considering their interactions. Tanaka *et al* quantitatively showed its formation mechanism from a unified numerical model taking account of thermal and dynamic interactions between the arc and the weld pool [7]. Furthermore, Yamamoto *et al* and Mori *et al* improved this model and additionally discussed the evaporation of the metal vapor from the weld pool and its diffusion in the arc[8,9]. However, fume formation mechanism from the metal vapor has not been reported in the arc welding.

This paper aims to clarify fume formation mechanism theoretically through visualization of fume shape. In this paper, a series of each process such as evaporation of metal vapor due to the arc and formation of fume from the metal vapor is totally discussed by numerical simulation which is calculated by coupling a GMA welding model which takes account of metal transfer with a fume formation model. Then, general mechanism of fume formation for arc welding process is discussed.

## 2. Simulation model

The simulation model employed in this study consists of a GMA welding model and a fume formation model. A metal vapor pressure and a cooling rate at a nucleation site are calculated by giving a welding condition to the GMA welding model. Then, the formations of primary particles and secondary particles are calculated by assuming the metal vapor pressure and the cooling rate as the calculation condition and the mechanism of fume formation can be discussed. The details of the simulation models are introduced as follows.

### 2.1 GMA welding model

The GMA welding model taking account of metal transfer process has been developed for coupling that with the fume formation model. **Figure 1** shows a simulation region consisting of an electrode wire, an arc and a base metal. The diameter of the electrode wire is 1.2mm and the thickness of the base metal is 10mm. The chemical compositions of the electrode wire and the base metal are pure iron. The arc length is 5mm with the DCEP (DC Electrode Positive) polarity. An arc current of DC200A is applied inside the electrode wire on the top boundary and the potential of the bottom boundary is set to be 0V. Argon gas is introduced as the shielding gas from the top boundary at the flow rate of 10L/min. The length of the electrode wire is 30mm in the initial condition. It is assumed that the electrode wire above the position of 29.4mm from the top boundary is always in solid phase and that below this position is in liquid phase. The droplet can be formed at the tip of the electrode wire with a balance among its surface tension, gravity and electromagnetic pinch force, and then can be also detached from the tip of the electrode wire to the base metal, which is called metal transfer. In the calculation of the droplet temperature, energy loss due to the latent heat for evaporation of the metal vapor was taken into account. The Volume of Fluid (VOF) method is used for the calculations of formation, detachment and transfer of the droplet. The region of the electrode wire is assumed to be initialized after the metal transfer immediately. In this model, time-dependent calculation is conducted for treating the metal transfer dynamically and ended at a time corresponding to the duration of 2 cycles of the metal transfer.

Governing equations consist of conservation equations of mass, momentum, energy, and current. The governing equations and the boundary conditions used in this simulation are the same as those in Ref [10]. A mass conservation equation is applied to take a metal vapor behavior into account as expressed in the below equation[11]. Only iron vapor is taken into account because the anode material employed in this study is made of pure iron.

$$\frac{\partial}{\partial t}(\rho C_1)+\frac{1}{r}\frac{\partial}{\partial r}(r\rho v_r C_1)+\frac{\partial}{\partial z}(\rho v_z C_1)= \frac{1}{r}\frac{\partial}{\partial r}\left(r\rho D\frac{\partial C_1}{\partial r}\right)+\frac{\partial}{\partial z}\left(\rho D\frac{\partial C_1}{\partial z}\right) \quad (1)$$

Where $\rho$ is mass density, $v$ is flow velocity, $C_1$ is mass fraction concentration of metal vapor and $D$ is the diffusion coefficient which is expressed by the viscosity approximation equation[12]:

$$D=\frac{2\sqrt{2}\left(1/M_1+1/M_2\right)^{0.5}}{\left[\left(\rho_1^2/\beta_1^2\eta_1^2M_1\right)^{0.25}+\left(\rho_2^2/\beta_2^2\eta_2^2M_2\right)^{0.25}\right]^2} \quad (2)$$

where, $M_1$ and $M_2$ are the molecular weights of iron and the shielding gas, respectively. $\rho_1$, $\rho_2$ and $\eta_1$, $\eta_2$ are the density and viscosity of iron and the shielding gas, respectively. $\beta_1$ , $\beta_2$ are the dimensionless constants defined as $\beta_i=\left(D_{ii}\rho_i\right)/\eta_i$ and theoretically range between 1.2 to 1.543 for various kinds of gas such as Ar, He, $H_2$, $N_2$, $O_2$ and $CO_2$. $\beta_1=\beta_2=1.385$ is assumed based on the mean value of the experimental data[12]. The viscosity approximation is acceptable up to 30,000K[13] because viscosity which is calculated as a plasma property takes ionized matters into account, and then it is considered to be suitable for modeling welding arcs.

On the anode surface (BE) where the temperature is

above the melting point, $C_1$ is given as[11]:

$$C_1 = \frac{p_{v,1}M_1}{p_{v,1}M_1 + (p_{atm} - p_{v,1})M_2} \quad (3)$$

where, $p_{atm}$ is the atmospheric pressure, and $p_{v,1}$ is the partial pressure of metal vapor which is a function of the weld pool temperature[14]. According the above equation, $C_1$ varies between zero and 1.0. For the other boundary conditions, $C_1$=0 at AF and FE shown in **Fig 1,** and $(\partial C_1/\partial r)=0$ at the arc axis (AB).

In the present model, plasma properties are dependent on not only the temperature but also the mole fraction of metal vapor. The plasma properties at the intermediate concentrations of metal vapor are calculated using a linear approximation based on the properties at 0, 1, 10, 20 and 30 mol% of metal vapor mixture rate[15]. The properties were calculated using the Chapman-Enskog approximation[15] under the assumption that the arc plasma is in a local thermodynamic equilibrium (LTE) condition. All of electron temperature, ion temperature and heavy particle temperature are the same in the LTE condition. The governing and auxiliary equations were solved iteratively by the SIMPLEC numerical procedure[16].

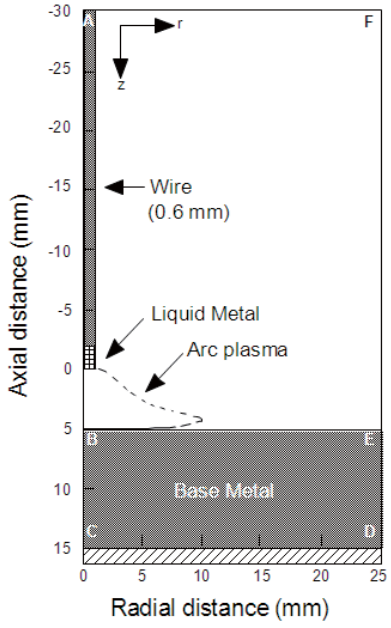


**Fig. 1** Schematic illustration of simulation domain for GMA welding.

2.2 Fume formation model

A simulation model for discussing the fume formation mechanism has been developed. In this model, the assumptions (1)~(5) are employed.

(1) The formation of supersaturation of the iron vapor by cooling.
(2) The formation of the primary particle by the homogeneous nucleation.
(3) The growth of the primary particle by the heterogeneous condensation.
(4) The formation of the secondary particle by the coagulation.
(5) The growth of the secondary particle by the heterogeneous condensation and the coagulation.

2.2.1 Homogeneous nucleation model of primary particle

In this paper, Friendlander's liquid-drop model in which all the nucleuses are assumed to be generated in liquid phase is employed[17]. In theory, the homogeneous nucleation can arise if the degree of supersaturation exceeds 1. It is assumed that the nucleus with a critical diameter $d_{pcri}$ is generated due to the nucleation. The critical diameter is the smallest nucleus's diameter and a nucleus can exist stable if its diameter is larger than the critical diameter which is represented by the equation (4).

$$d_{pcri} = \frac{4\sigma_p v_m}{kT \ln S} \quad (4)$$

where $\sigma_p$ is surface tension, $v_m$ is volume of the iron atom, k is the Boltzmann constant, $T$ is temperature, $S$ is degree of supersaturation. The homogeneous nucleation rate $J$ which is the number of nucleuses generated per unit volume and unit time is written as[18]:

$$J = N\frac{\zeta n_1}{12}\sqrt{\frac{\Theta}{2\pi}}\exp\left[-\frac{4\Theta^3}{27(\ln S)^2}\right] \quad (5)$$

Where $N$ is a normalization constant written by equation (6). The Brownian collision between iron atoms. $\zeta$ is represented by the equation (7) which is applicable if Knudsen number is more than 10. This value becomes 1000 at least through this simulation. The $n_l$ is number density of iron atoms. $\Theta$ is a dimensionless surface energy expressed by equation (8).

$$N = n_s \exp\Theta \quad (6)$$

$$\zeta = 4\left(\frac{3v_m}{4\pi}\right)^{1/6}\sqrt{\frac{12kT}{\rho}} \quad (7)$$

$$\Theta = \frac{\sigma_p s_1}{k\ T} \quad (8)$$

Where $n_s$ is the iron atom concentration for the saturated vapor, $v_l$ is volume of the iron atom and $s_1$ is surface area of the iron atom.

2.2.2 Heterogeneous condensation model of primary particle

When the particle growth is governed by the heterogeneous condensation of the vapor, an equation for the growth rate $G$, which is change in diameter per unit time, expressed below can be obtained from a material balance over the growing particle and is represented by the following equation[19].

$$G = \frac{4}{d_p}\frac{R_g}{R_c} D_g \left(X - X_s\right)\left\{\frac{1+K_n}{1+1.7K_n+1.333K_n^2}\right\} \quad (9)$$

Where $R_g$ and $R_c$ are the molar densities of the gas phase and the condensation phase, respectively. $D_g$ is diffusion coefficient defined as $\lambda\overline{v}/3$, $\lambda$ is mean free path of iron atoms, $\overline{v}$ is mean speed of iron atoms[20]. $(X\text{-}X_s)$ represents difference of gas-phase mole fraction and equilibrium state mole fraction. $K_n$ is the Knudsen number defined as $K_n=\lambda/(d_p/2)$.

2.2.3 Coagulation model of secondary particle

The primary particles generated by the nucleation grow up through not only the condensation of iron atoms but also the coagulation caused by collisions between particles. In this model, the coagulation process is calculated by analyzing movements and collisions of particles distributed in the simulation region. A two-dimensional simulation region for the coagulation model is defined for time shorting. The size of the region is determined by the number density of primary particles obtained from the primary particle model to include 1000 particles in the region. The three dimensional number density of primary particles determined by the primary particle model is converted into the two dimensional number density by raising it to the 2/3th power. Secondary particles with various shapes and sizes are formed in the arc welding because the formation is very stochastic. However, only several or several tens of secondary particles are analyzed as examples of the formation in this simulation due to the limitation of the computational resource.

When the nucleation occurs, a primary particle is posted at a random position in the region and an initial velocity with a random direction is given to the particle. The initial velocity is determined from the thermal velocity calculated from the surrounding plasma temperature. The sum of the momentums is conserved through a particle collision. If particles collide at temperature above the melting point, they fuse into one spherical particle conserving their volumes. In other case, they attach each other like a chain shape depending on the temperature comparing with the melting point. A particle escaped from a boundary of the region is injected from the opposite boundary with the same velocity vector.

2.2.4 Calculation conditions

As described below, the nucleation occurs around 2,000K in this calculation condition. Therefore, the initial temperature is set to be 3,000K as that in the upstream region. The temperature decreases by 0.5K until the room temperature of 300K. The homogeneous nucleation model, the condensation model and the coagulation model are solved in each temperature step. It is required to provide the metal vapor pressure and the cooling rate obtained from the GMA welding model to the fume formation model as the initial conditions. The metal vapor pressure is referred from the value in the region at 3,000K. The cooling rate is calculated as product of temperature gradient and plasma flow velocity at 2,000K. Because these values depend on positions and should be averaged spatially in the corresponding regions.

## 3. Results and discussion

**Figure 2** shows temperature distributions at t=12ms, 14ms, 16ms, and 20ms in the second cycle of the metal transfer in GMA welding. It can be seen that a droplet is formed at t=12ms, and then detached from the tip of the electrode wire at t=14ms, and finally it was transferred to the weld pool at t=20ms. The droplet temperature peaked immediately before the detachment (t=12ms) and became more than 3,000K near the under surface of the droplet because the droplet was heated by the electron condensation and the thermal conduction from the arc covering the droplet whose temperature reached 16,000K. There was large temperature gradient in the droplet because the temperature near the constricted part of the electrode wire was approximately 2,500K. On the other hand, the maximum weld pool temperature was only 2,400K.

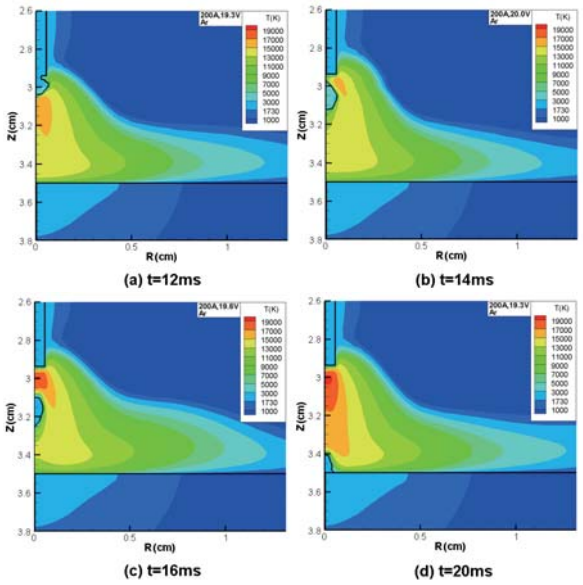


**Fig. 2** Time variation in temperature distribution in argon GMA welding.

**Figure 3** shows distribution of metal vapor pressure. The metal vapor was evaporated mainly from the droplet and the tip of the wire. The metal vapor pressure became approximately 26,000Pa in the maximum near the droplet. On the contrary, it was found that the metal vapor pressure near the weld pool surface was relatively low because amount of the metal vapor evaporated from the weld pool was weak. This difference is caused by higher temperature of the droplet compared with that of the weld pool. The metal vapor was swept away in radial direction through the region close to the base metal surface due to the plasma flow similar to the case in the GTA welding.

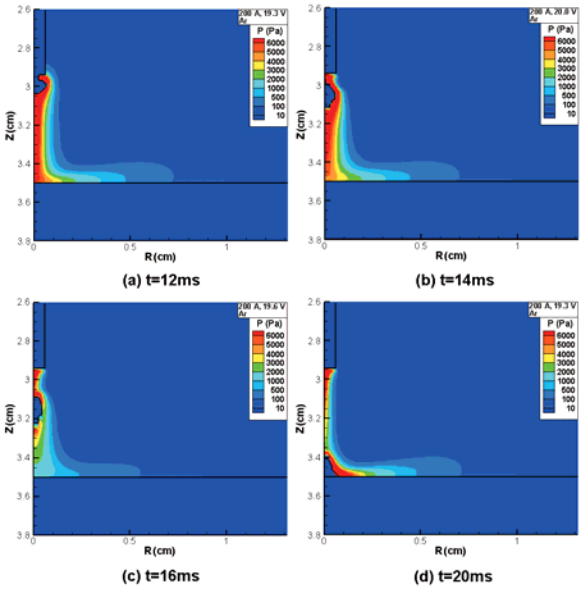


**Fig. 3** Time variation in metal vapor pressure distribution in argon GMA welding.

The metal vapor pressure and the cooling rate as initial conditions of the fume formation model were determined from results at t=12ms when the metal vapor pressure reached the maximum. In the present study, the fume characteristics in three positions classified in the feature as shown in **Figures 4 and 5** were examined. In position 2, the metal vapor was swept away outward due to high speed plasma flow, and therefore metal vapor pressure was low. In position 3, the metal vapor pressure was higher than that in position 2 because of the sum of evaporation from the weld pool surface and compression due to the plasma flow from the electrode wire. Since this model assumes rotational symmetry around the arc axis, the droplet transfers along the central axis. However, in practice metal transfer tends to be unstable by various factors such as the arc pressure on the side under the droplet. Therefore, the possibility of the metal vapor near the droplet diffusing directly to the surroundings of the arc without getting on the plasma flow should be considered. Assuming such a situation, the metal vapor pressure near the droplet and the cooling rate in the edge of the arc column adjacent to the droplet were provided in position 1. The cooling rates in position 1, 2, and 3 were $1.1\times10^5$, $5.0\times10^5$ and $1.0\times10^5$K/s, respectively. The metal vapor pressures in each position were 26,000, 4.5 and 100Pa.

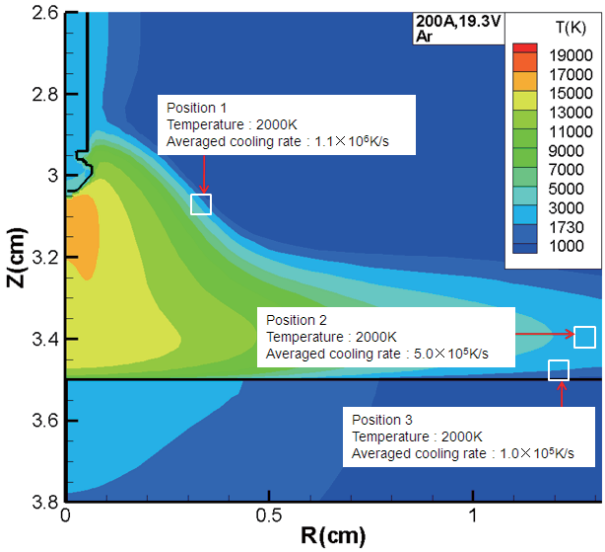


**Fig. 4** Distribution of temperature at t=12ms in argon GMA welding.

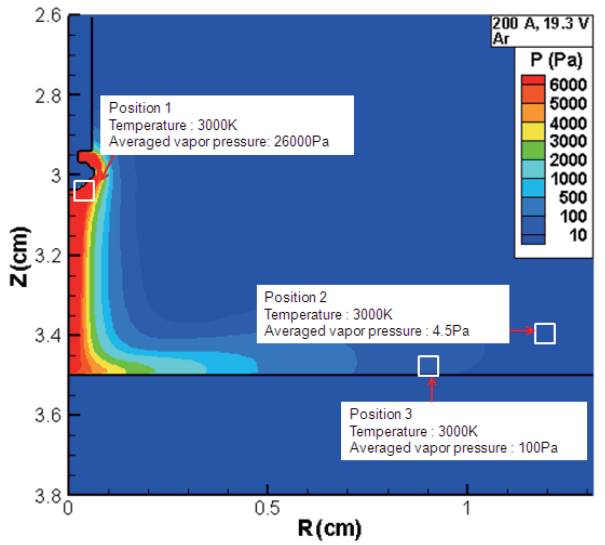


**Fig. 5** Distribution of metal vapor pressure at t=12ms in argon GMA welding.

**Figure 6** shows dependences of metal vapor pressure and saturated pressure on temperature in the same manner with **Fig 5**. In position 1, 2, and 3, the metal vapor was consumed at 2400,1200 and 1600K, respectively. It was found that nucleation and the condensation occurred at higher temperature with higher metal vapor pressure provided as initial conditions.

The sizes of the regions of the coagulation model were $210\,\mu$m$\times210\,\mu$m,$10\,\mu$m$\times10\,\mu$m and $56\,\mu$m$\times56\,\mu$m in position 1, 2, and 3, respectively. In position 1, large amount of particles existed in the region and the size of the particle reached several μm in the maximum at 300K. Only one secondary particle and three secondary particles were formed in positions 2 and 3.

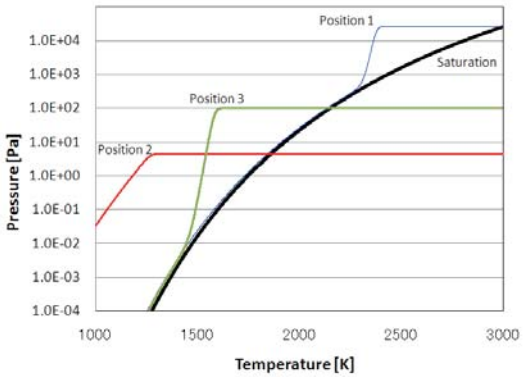


**Fig. 6** Dependence of metal vapor pressure on temperature in argon GMA welding.

**Figure 7** shows dependences of number densities of primary particles and secondary particles on temperature. In each position, the number density of primary particles began to decreases after the maximum due to the coagulation through collisions among primary particles instead of increase of secondary particles. With further decreasing of the temperature, the number density of secondary particles also decreased because of the coagulation among them. The change in number density by the coagulation was more gradual for position 1 than other positions, and thus high number density was maintained also in 300K. It is considered that the collision frequency decreases because the nucleation occurs above the melting point of iron and then size of particle, which affects collisional cross-section, hardly grows up due to fusion in the collision.

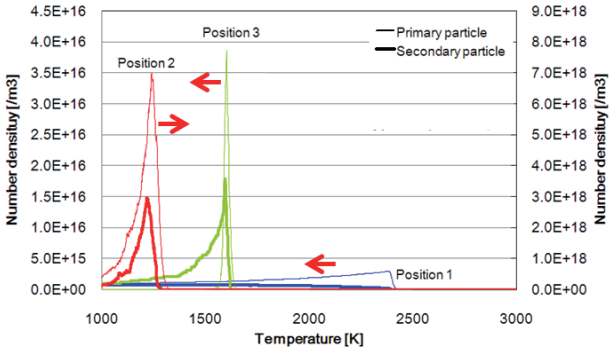


**Fig. 7** Dependences of number densities of primary and secondary particles on temperature in argon GMA welding.

**Figure 8** shows magnifications ($4\mu m \times 4\mu m$ for position 1, $100nm \times 100nm$ for position 2, $500nm \times 500nm$ for position 3) of examples of secondary particles at 300K. Large spherical particles with sizes of several hundreds nm were observed in position 1. It is suggested that the particle grows up due to the influence of fusion in the coagulation in addition to high metal vapor pressure near the droplet. On the other hand, in position 2 a number of primary particles with size of several nm constituted a secondary particle with size of several tens nm, because the coagulation occurred under the melting point and the metal vapor pressure was low in this position. In position 3, it can be seen that primary particles with size of several tens nm joined like a chain and constituted the secondary particle with size of 500nm. For a reason, it is considered that the metal vapor pressure increases near the weld pool surface because of the sum of metal vapor evaporated from the weld pool and that transported from the droplet by the plasma flow.

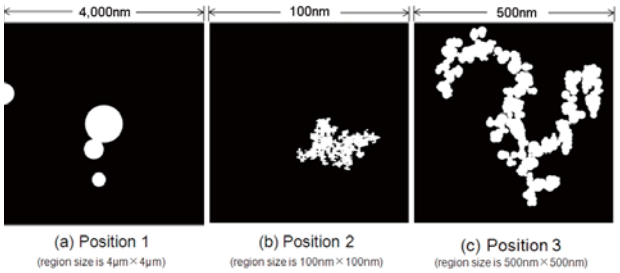


**Fig. 8** Shapes of secondary particles at 300K in case of position 1 (region size is $4\mu m \times 4\mu m$), position 2 (region size is $100nm \times 100nm$) and position 3 (region size is $500nm \times 500nm$).

**Figure 9** shows typical experimental examples of the fume shape in GMA welding with different three types of shielding gas compositions, namely, MIG($Ar+2\%O_2$), $CO_2$ and MAG($Ar+20\%CO_2$). It is found that particles with size of several tens nm join like a chain and constituted a secondary particle with size of several $\mu m$ in MIG. In $CO_2$ and MAG, these particles grow up like a spider's web. Furthermore, small number of large particles with size of several hundreds nm exist as marked in **figure 9**. These kinds of particles are found especially in $CO_2$. In case of MIG in which the metal transfer is smooth and stable, particle shape is similar to that in positions 2 and 3 of simulation results as shown in **Figs 8 (b) and 8 (c)**. It is expected that large part of the fume was produced by the metal vapor evaporated from the electrode wire, the droplet and the weld pool through the downstream region of the arc. On the contrary, since the arc was constricted by high specific heat of $CO_2$, namely, *the thermal pinch effect*[21], the arc pressure lifting the droplet increases in $CO_2$ and MAG welding. Consequently, the droplet tends to grow largely and the whole surface of the droplet can be hardly covered by the arc. It is suggested that the disturbance of the metal transfer leads to direct diffusion and quenching of the metal vapor without a path through the downstream region of the arc. Therefore, the fume with size of several hundreds nm can be produced specially in $CO_2$ as shown in simulation results in position 1 in **Fig 8 (a)**.

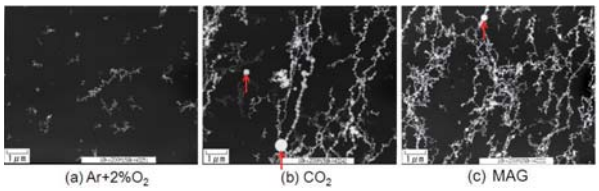


**Fig. 9** Fume shapes obtained by TEM observation in MIG, CO2 and MAG welding.

As explained above, it was shown that most part of the fume was produced in downstream region of the arc originating from the metal vapor evaporated mainly from the droplet by employing the GMA welding model. This kind of the fume was constituted of particles with size of several tens nm and has similar characteristics to that of GTA welding. On the other hand, if the metal transfer becomes unstable and the metal vapor near the droplet diffuses directly toward the surroundings of the arc not getting on the plasma flow, the size of particles reaches several hundreds nm. This tendency agrees with morphological shape of fume in $CO_2$ and MAG obtained from experimental observations.

In this study, fume formation was assumed in inert gases such as argon and helium. However, in the future, it will be necessary to consider the influence of the oxidation in the fume formation, because the air containing oxygen will exist actually in the surroundings of the arc. The effects of metal transfer modes, such short arc or spay mode on fume formation and the effect of process parameters, such as welding current, arc length, flow rate of shielding gas on fume formation should be studied in the future because those are important for understanding the fume formation mechanism essentially. The information obtained through this study will contribute to develop an electrode wire and to optimize welding conditions for reducing the fume.

## 4. Conclusions

Main conclusions are summarized as follows:

1) Most part of the fume was produced in downstream region of the arc originating from the metal vapor evaporated mainly from the droplet in argon GMA welding. This kind of the fume was constituted of particles with size of several tens nm.
2) If the metal vapor near the droplet was assumed to diffuse directly toward the surroundings of the arc not getting on the plasma flow, the size of particles reaches several hundreds nm in GMA welding. This tendency agreed with the fume shape in $CO_2$ and MAG obtained from experimental observations.

References

1) Terasaki H, Tanaka M and Ushio M 2002 Metall. mater. trans. A 33 1183-1188
2) Kobayashi M, Maki S, Hashimoto Y and Suga T 1980 Journal of the Japan Welding Society, 49 454-461
3) Jenkins N T and Eagar T W 2005 Welding Journal 84 87-s
4) Bosworth M R and Deam R T 2000 J. Phys. D: Appl. Phys. 33 2605-2610
5) Watanabe T, Atsuchi N, and Shigeta M 2007 Thin Solid Films 515 4209-4216
6) Schmid H J, Al-Zaitone B, Artelt C and Peukert W 2006 Chemical Engineering Science 61 293-305
7) Tanaka M and Lowke J J 2007 J. Phys. D: Appl. Phys. 40 R1-R23
8) Yamamoto K, Tanaka M, Tashiro S, Nakata K, Yamazaki K, Yamamoto E, Suzuki K and Murphy A B 2009 Quarterly J. Japan Welding Soc. 27 4s-7s (in Japanese)
9) Mori Y, Iwao T, Yumoto M, Tashiro S and Tanaka M 2009 Quarterly J. Japan Welding Soc. 27 8s-12s (in Japanese)
10) Yamamoto K, Tanaka M, Tashiro S, Nakata K, Yamazaki K, Yamamoto E, Suzuki K and Murphy A B 2008 Sci. & Tech. Welding & Joining 13 566-572
11) Menart J and Lin L 1999 Plasma Chem. & Plasma Process. 19 153-170
12) Wilke C R 1950 J. Chem. Phys. 18 517-519
13) Murphy A B 1996 J. Phys. D: Appl. Phys. 29 1922-1932
14) The Japan Institute of Metals 1993 Edition No. 3 Data Book of Metal (MARUZEN CO., LTD) (in Japanese).
15) Murphy A B 1995 Plasma Chemistry and Plasma Processing 15 279-307
16) Patanker S V 1980 Numerical heat transfer and fluid flow (Hemishpere Publishing Corporation)
17) Friendlander S K 1983 Annals of the New York Academy of Sciences 404 354
18) S. L. Girshick, C. P. Chiu and P. H. McMurry: Time-Dependet Aerosol Midels and Homogeneous Nucleation Rate, Aerosol Sci. Tech,13:4 (1990), 465-477.
19) Joshi S V, Liang Q, Park J Y and Batdorf J A 1990 Plasma Chem. Plasma Process 10 339-358
20) Fuchs N A and Sutugin 1971 "Topics in Current Aerosol Research" International Reviews in Aerosol Physics and Chemistry, Vol. 2 (PergamonPress)
21) Murphy AB, Tanaka M, Yamamoto K, Tashiro S, Sato T and Lowke JJ 2009 J. Phys. D: Appl. Phys. 42 194006